EG UK Computer Graphics & Visual Computing (2024)
A. Slingsby and D. Hunter (Editors)

Investigation of the organisation of the extracellular matrix using fibre tracing

Y. Arafat[1], C.Cuesta-Apausa[2], E. Castellano[2] and C.C. Reyes-Aldasoro[1]

[1]Department of Computer Science, School of Science and Technology, City, University of London, UK
[2]Tumour-Stroma Signalling Lab, Universidad de Salamanca, Salamanca, Spain

Abstract

Throughout history, the observation of medical and biological samples has been of high importance and has led to many discoveries. When this process relies on human observation, it can be time-consuming, especially with the advent of technological advancements that generate more and more images at faster rates. Additionally, some features of the samples can be undetectable by the naked eye, but with the aid of visual computing techniques, these hidden details can be revealed. The morphological characteristics of the extracellular matrix play a vital role in cancer and other health conditions. Visual observations of the ECM can provide valuable insights; however, the task may be tedious and sometimes it is hard to quantify the differences between samples. In this work, a tracing algorithm is proposed. Furthermore, morphological characteristics of the extracellular matrix can be extracted with the algorithm to quantify and compare different biological populations. Experiments revealed that the removal of interactions in fibroblasts affected their ability to form a healthy extracellular matrix as compared with a wild type population. Here, an investigation of the morphological differences between the ECM of two populations was conducted. Five images of mutant and five images of wild type cells growing in culture were compared. A deconvolutional convolutional neural network was used as a pre-processing filtering method to remove noise from the images. The images are then traced by the proposed algorithm, Trace Ridges, to extract morphological features and visually present the edges and gaps extracted. Trace Ridges combines methods of Edge detection, watershed, and morphological characteristics to delineate fibre-like structures. Two morphological characteristics provided statistical differences between the populations: number of fibres ($p-value = 0.00091$) and relative area of gaps between the fibres ($p-value = 0.014$). The number of fibres detected in wild type was higher than mutant while the relative gaps area size of mutant was higher than that of WT. Trace Ridges was able to successfully delineate the ECM fibres of mutant and wild type cells and extract morphological features to show the difference between the populations.

CCS Concepts

• ***Computing methodologies*** → ***Object detection;***

1. Introduction

The observation of medical and biological samples has been crucial in many scientific discoveries, from the discoveries of microorganisms and cell structures observed by Hooke and Leeuwenhoek [Ges04] to the discovery of the neural networks and retinal arrangements by Santiago Ramon y Cajal [Ber94]. Traditionally, these samples have been observed and analysed by humans, with their extraordinary vision and brain power. However, with advances in technology, these experiments now provide far too many images for a single individual to process in a reasonable time frame. In addition, sometimes datasets may contain characteristics that are too subtle for human eyes to perceive and the application of visual computing techniques can reveal interesting features that would otherwise remain hidden. Thus, these images of medical and biomedical experiments are now considered as digital images, the data these images contain can be processed into graphics that can be then interpreted with computing algorithms that can enhance a visual observation or can extract automatically characteristics of the data.

Morphological attributes of cells have been widely studied, particularly in the context of cancer [ACQ*20, MSMB21, WPK*15] and other conditions of health and disease [HLHL22]. However, there is a growing acknowledgment of the impact the microenvironment that surrounds these cells and influences the development or progression of the disease [FDMJ10] [MWCU20] [YCH*24]. In particular, the extracellular matrix (ECM) plays a vital role in the evolution of cancer [PJ22, WAOMW20, HZW*21, WM-

DOI: 10.2312/cgvc.20241238

DRH18, PMFT02] and other health conditions [IG18]. Yet, the extracellular matrix has been widely overlooked [FCC18] in comparison to other factors such as vasculature, macrophages and soluble factors. A potential cause of this dismissal could be due to the intricate three-dimensional architecture [Yue14, PLG*21] of the ECM, which is composed of an array of elements including glycoproteins, collagen and enzymes. Understanding the structural properties of these glycoproteins can yield valuable insights especially through the application of computer vision and visualisation techniques.

In vitro experiments have revealed how certain modifications of the DNA sequence of cells i.e., creating mutant cells, can provide completely different characteristics and interaction between cells. In this paper we investigate how mutant fibroblasts compare against wild type fibroblasts in the formation of the extracellular matrix.

Whilst visual examinations of the extracellular matrix structure can unveil compelling properties, relying solely on such observations can prove challenging to compare populations. Analysing structural properties of the ECM, such as the shape, distribution, and count of the fibrial glycoproteins, could offer valuable insights into the microenvironment or treatment effects. Quantifying these fibres will showcase their properties.

Several methodologies for tracing have been proposed. Edge detection [Can86], Scale Space [Lin98b, Lin98a], Watershed algorithms [Mey92, Mey94], CT Fire algorithm [BLP*14, LKP*20], Twombli [WPB*21], Graph Based [GEOS*23, Gra20] and deep learning architectures have been widely used like the well-known U-Net [RFB15]. In a recent comparison [ACACRA24], Trace Ridges proved to be the most robust and accurate algorithm for tracing fibre-like structures.

The main contributions of this work are the application of Trace Ridges as a visual computing technique to extract and visualise biological differences in the extracellular matrix produced by mutant and wild type fibroblasts. By leveraging Trace Ridges as a visual analysis tool, this work highlights the distinct patterns that differentiate the biological processes in these cell types.

Trace Ridges follows a pipeline of traditional image processing steps, and it can successfully delineate the fibres of the ECM and statistically distinguish between mutant and wild type experiments. Furthermore, it is simple and fast and outperformed all other methodologies in accuracy.

2. Material and Methods

2.1. Data sets

Mutant/Wild Type (WT) cell preparation and acquisition has been explained in [GRH*07]. p110α mutant and wild type fibroblasts were cultured on a gelatin coated surface treated with glutaraldehyde. This facilitates extracellular matrix formation. Subsequently, five sets of fluorescent images were obtained for both mutant and WT samples to assess fibronenctin expression (Fig. 1).

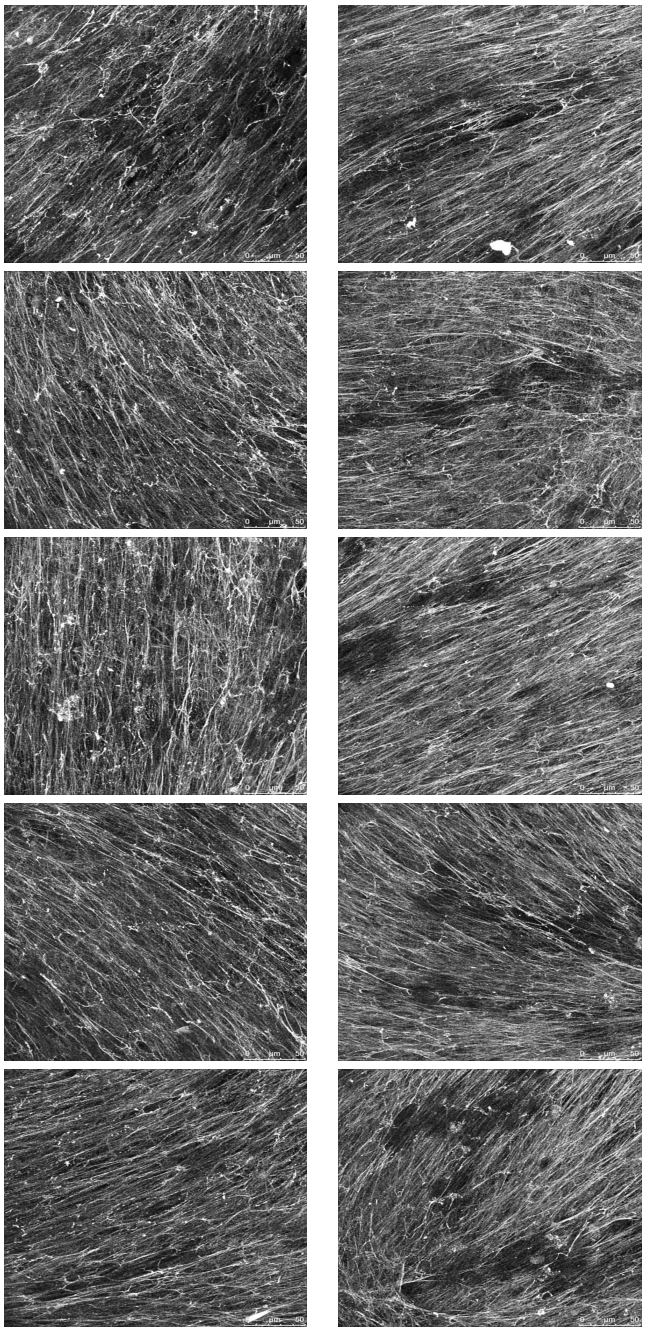

(a) (b)

Figure 1: *Illustration of various images of the extracellular matrix fibronectin. (a) Images representing mutant cases. (b) Images representing wild types. It should be noticed the complexity of the fibres that create the extracellular matrix and the difficulty to analyse these by pure observation.*

2.2. Pre-processing image filters

In the field of image processing, filters are commonly used to modify an original image into a new image in which the filter has altered the data. Filters can enhance a relevant feature of the data or

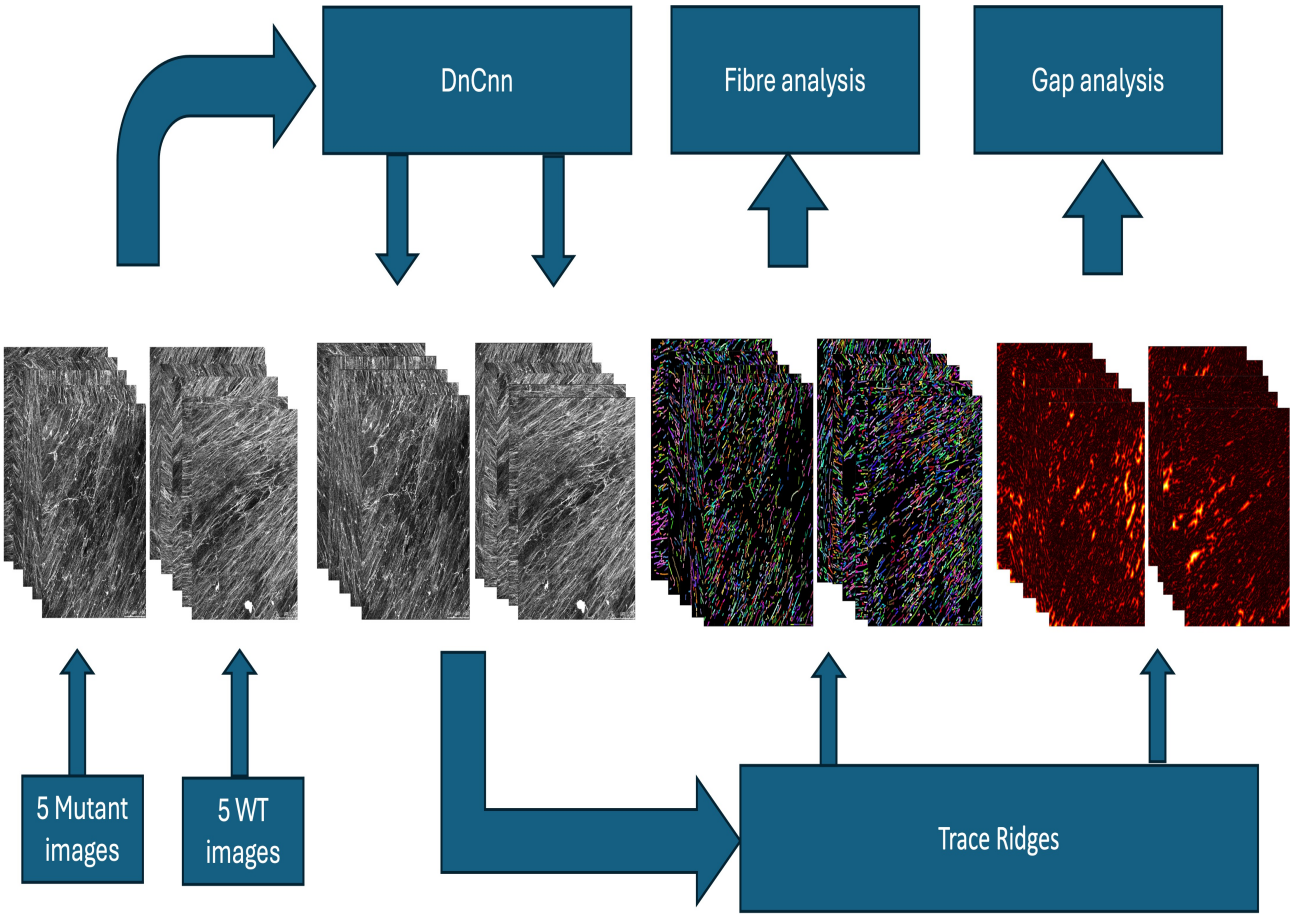

Figure 2: *Implementation pipeline of Trace Ridges. Fluorescent fibronectin images are run through DnCnn for filtering then they are passed to Trace Ridges. Labelled fibres and distance maps are produced where fibre and gap analysis could be carried out respectively.*

suppress an unwanted characteristic, for instance noise. There are many types of filters [RH99], of which the most common are the spatial filters, which multiply the value of the pixels of a region of the image with a small kernel or filter, the filter is then moved along the image and the process repeated until all the image has been multiplied and a new image is produced.

Alternatively, frequency or Fourier filters convert the image into the frequency domain or frequency domain through the Fourier Transform [Bra78] (or another transform like Wavelet or Cosine) and then apply frequency filters on the Fourier domain, apply an inverse transform to reconvert the result of the process to the spatial domain. The filter function shape varies depending on the purpose of use. Filters can suppress the high frequencies of an image and smooth the image and reduce noise or they can suppress the low frequencies of an image to enhance the edges in an image. A common frequency filter function is the Gaussian filter.

Filters have been used in many imaging domains for various cases such as facial images [HS16] or MRI denoising [SV17]. Furthermore, with the ever-evolving field of artificial intelligence, deep convolutional neural networks [II21] can be trained to remove noise from noisy images and be comparative to the more traditional filtering methods. In the recent comparison [ACACRA24], three methods of preprocessing filtering were used and DnCnn a denoising deep convolutional neural network was superior in its filtering performance on fluorescent fibronectin images.

2.2.1. DnCnn filter

DnCnn [ZZC*17] represents a deep convolutional neural network designed specifically for de-noising noisy images. Employing residual learning and batch normalisation, this model effectively removes noise from the input noisy observations. Notably, DnCnn demonstrates proficiency in handling blind Gaussian de-noising with unknown noise level. Training of the DnCnn model utilised a dataset compromising of images of fibre-like structures that are publicly available and found in [BLP*14, LKP*20, GEOS*23, WPB*21]. The images were split into two halves, with one portion allocated for training and the other unseen. When necessary, images were converted to 2-D grayscale to align with the model's input requirements. Training parameters included a learning rate of 0.001 and a batch size of 32.

2.3. Tracing algorithm

The Trace Ridges algorithm was selected for fibronectin tracing and morphological analysis due to its superior performance compared to six other tracing algorithms. Some algorithms, like Scale Space and Edge detection, are general and can be applied for various tasks beyond fibre tracing. Others such as CT Fire, Twombli and Graph based methods, are specifically designed for fibre tracing. U-Net a deep learning architecture was also included in the comparison, capable to segment any objects all it requires is training images and patches. Ultimately, Trace Ridges demonstrated the lowest total distance error with 165,873 pixels compared to the second-best Graph based method with 200,687 pixels. Total distance error is a measurement of the total pixels in an image the algorithm trace was from the manually delineated ground truth. Furthermore, it exhibited the second lowest average distance errors with 9.27 pixels after Edge detection with 9.1 pixels, but it is argued that it performs best for this metric due to Edge detection's nature to over-segment and trace two edges for a fibre. The average distance error is a measurement of the average number of pixels one fibre trace was far from the ground truth in an image. Finally, Trace Ridges had the fastest computational processing time of 2.45s after Edge detection with 0.467s, with the next algorithm UNET being five times slower with 14.13s. Additionally, in this study, three pre-processing filters were applied to deal with noise. The three filtering options were, no filtering, low pass Gaussian filtering and Deconvolutional convolutional neural network (DnCnn). Pre-processing with DnCnn filtering notably reduced distance errors for fluorescent fibronectin images. Total distance error with DnCnn was 162,760 pixels compared to 166,690 pixels with Gaussian filtering and 168,170 pixels with no filtering. Fibronectin images with DnCnn processed faster having just taken 2.9s compared to 3.1s and 4.0s with Gaussian and no filtering respectively. The Trace Ridges algorithm uses techniques of Edge detection, watershed, and morphological information to trace fibre-like structures. Trace Ridges extracts morphological and topological information including fibre length, fibre count, gap area and orientation and visually presents these observations. Overall, Trace Ridges emerged as the most robust algorithm.

2.3.1. Trace Ridges

Trace Ridges combines watershed [Mey92, Mey94] to find ridges. The Watershed algorithm views an image as a topographic surface where higher intensity pixels represent peaks and hills, and lower intensity pixels represent basins. The watershed algorithm begins by calculating the image gradient and selecting labels based on criteria such as local minima and maxima. It then floods the image, expanding regions around these labels to find the lowest points between them, forming watershed lines where regions meet. Watershed is combined with Edge detection. Edge detection [Can86], which breaks any ridges that run from a main ridge towards the sides of the basins and thus leaves the main ridge of a structure separate from minor ridges.

The Canny Edge detection [Can86], introduced by Canny in 1986, is utilised to detect object boundaries also known as edges within an image by identifying variations in pixel intensities. Initially, Gaussian filtering is employed to minimise noise, followed by non-maximum suppression to refine the detected edges. Thresholding, referred to as hysteresis, is then applied to determine which edges are retained or discarded. Trace Ridges uses a filter size of 2×2 of the Canny Edge detector to extract edges representing fibrous structures.

Trace Ridges then morphologically selects ridges for length and brightness, i.e., foreground pixels are those of higher elevation and the background pixels have low elevations and any ridges of low intensities are discarded. This strategy favours brighter, longer ridges, which produce cleaner results with fewer traces than other techniques. Finally Trace Ridges visually showcases the fibres delineation and gap analysis to support the metrics results.

Implementation of Trace Ridges is straightforward using the function "[fibronectinOut,fibronectinOut2,dataOut] = Trace_Ridges(dataIn)". Here "dataIn" is the input image. The output fibronectinOut lists extracted morphological features which include but not limited to the number of fibres detected, their orientation and gap analysis. fibronectinOut2 provides visual outputs including labelled detected fibres, a distance map that shows gaps of the input image and orientation maps. dataOut displays the detected fibres overlaid on the original image for verification. Trace Ridges required no other parameters other than the input image. An example of the implementation pipeline of Trace Ridges for the fluorescent fibronectin images is illustrated in (Fig. 2).

3. Results

3.1. Morphological comparison of Wild type and mutant ECMs

Images of the extracellular matrix of two groups (mutant, $n = 5$, WT $n = 5$) shown in (Fig. 1) and (Fig. 3a-b). The images were processed by Trace Ridges to trace the fibres. Subsequently, two morphological metrics were derived. Firstly, the count of delineated fibres was determined (Fig. 3c) and (Fig. 4), this is the number of edges detected by the algorithm. Secondly, a distance transform was computed that calculates the Euclidean distance of every pixel that is not part of an edge, referred to as "gaps", to its closest edge, and the relative area of the gaps was calculated. Brighter regions indicate greater distance from a fibre. The relative gap area was computed for each image (Fig. 3d) and (Fig. 5), representing the average of all gap sizes relative to the image size.

Boxplots for the two metrics is shown in (Fig. 6), in all cases there was statistical differences with $p - values$ of 0.00091 and 0.014.

The number of fibres detected in WT were higher than that of the mutant presented in (Table 1). The highest number for WT was 2363, while for the mutant is 1851. The lowest number of fibres detected for mutant was 1503 and for WT 1964. Therefore, the median of WT was higher than mutant. The WT possessed a larger range (Fig. 6). The lowest value of number of fibres detected in WT was greater than the highest value for the mutant. Visually by observing (Fig. 4), the mutant culture images (Fig. 4a), the fibres are more dispersed and spread out and are fewer in quantity in comparison to the WT (Fig. 4b) where the fibres appear to be tightly packed and are abundant. A higher number of fibres detected in the wild type extracellular matrix suggests that, biologically, it contains more fibres on average compared to the mutant fibroblasts.

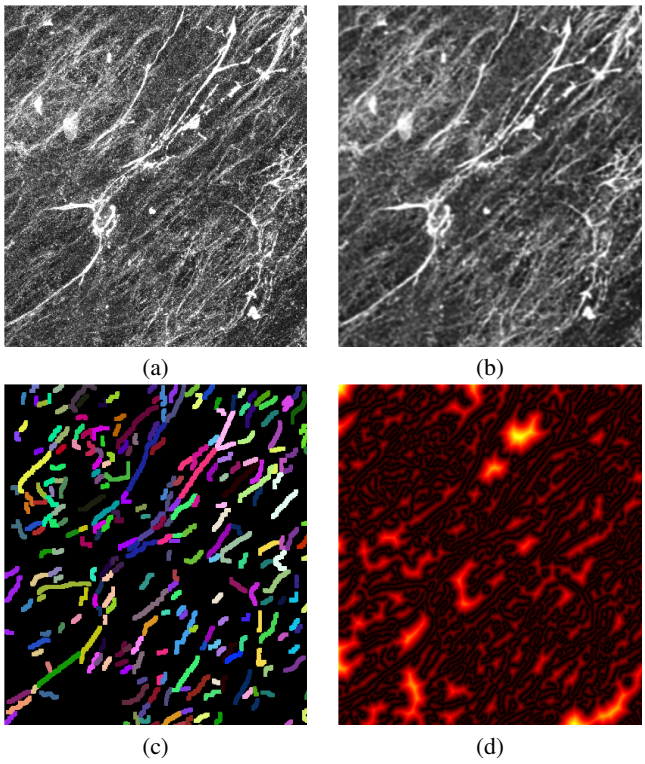

Figure 3: *(a) Fluorescent Fibronectin region of interest (ROI). (b) DnCnn application on Fluorescent Fibronectin (ROI). (c) Number of edges (ROI). Colours are randomly assigned. (d) Gaps between fibres (ROI). Brighter yellow means pixel is further away from an edge.*

	Num Edges	Rel Gap Area
Mutant_1	**1503**	**0.5461**
Mutant_2	**1677**	**0.5215**
Mutant_3	**1708**	**0.5542**
Mutant_4	**1536**	**0.5353**
Mutant_5	**1851**	**0.5385**
WT_1	**2084**	**0.5193**
WT_2	**2129**	**0.5095**
WT_3	**2363**	**0.4926**
WT_4	**2068**	**0.5278**
WT_5	**1964**	**0.5188**

Table 1: *Morphological analysis on five sets of mutant and WT images. Num Fibres is number of edges detected in an image. Rel Gap Area is the relative gap area size.*

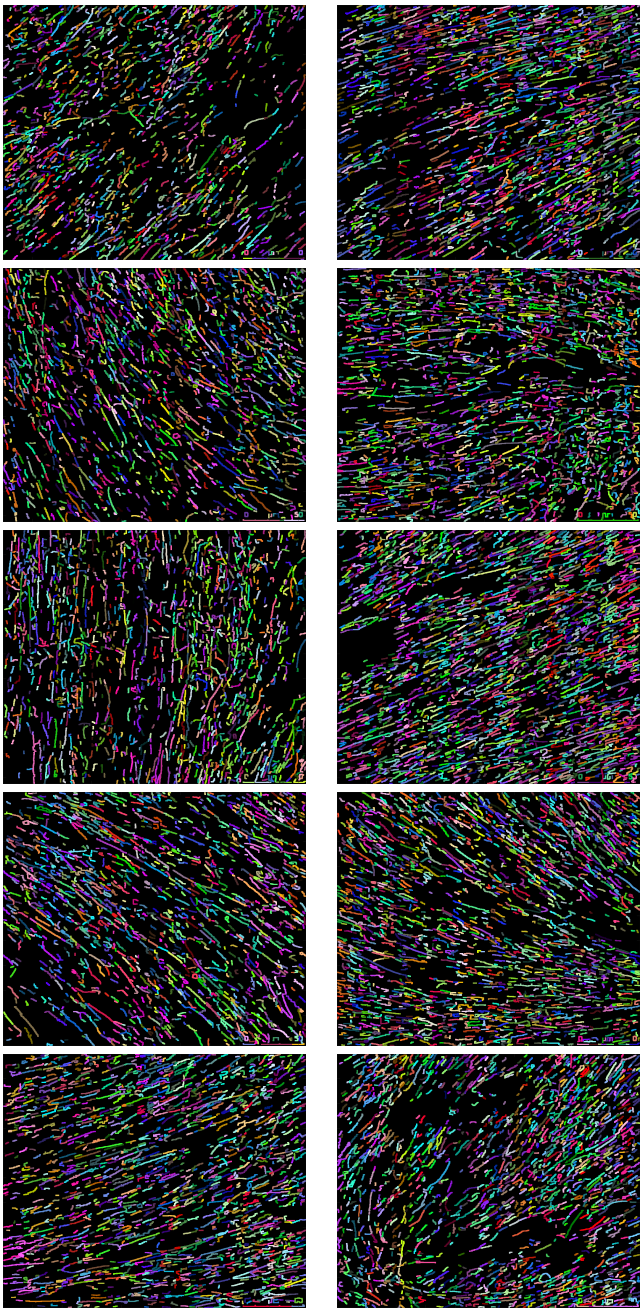

Figure 4: *Fibres detected by Trace Ridges. Colours are assigned randomly to distinguish different edges. (a) Images representing mutant. (b) Images representing WT. Black regions in the images are gaps between the fibres. Visually, the wild type extracellular matrix exhibits a higher fibre density with minimal gaps between the fibres. In contrast, the mutant fibres appear more dispersed, with the images showing significantly larger gaps between them.*

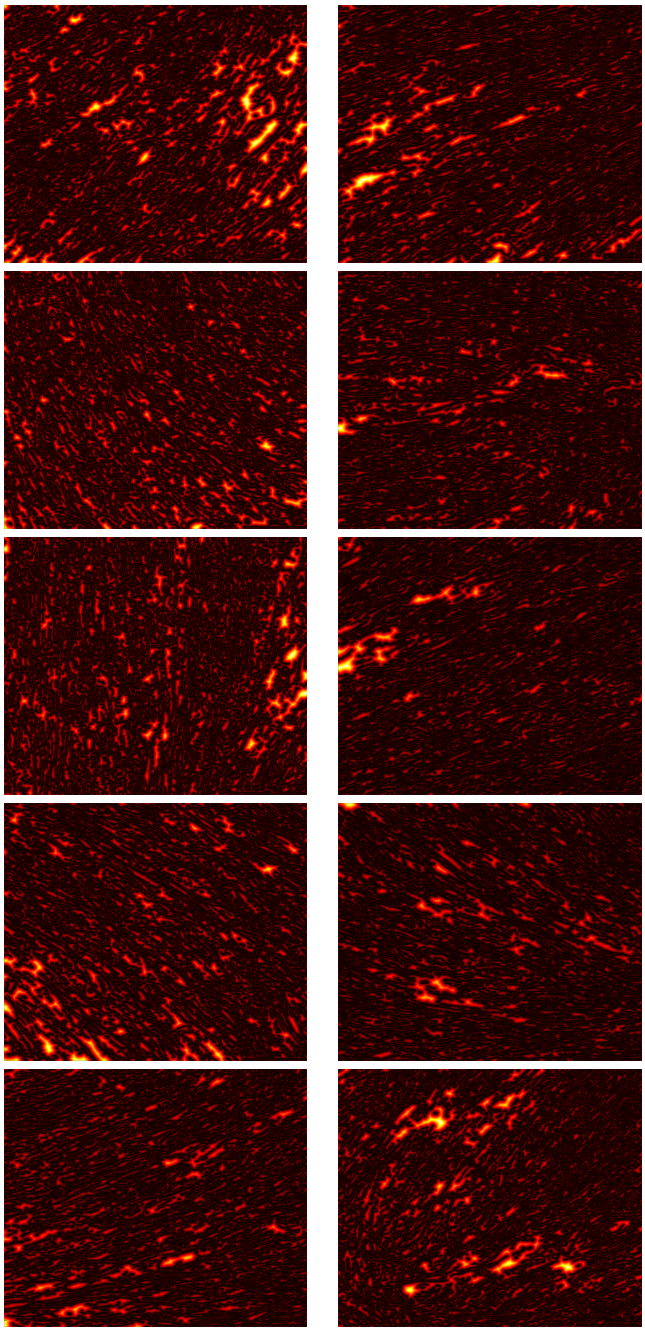

(a) (b)

Figure 5: *Relative gap area size. Brighter yellow regions indicate pixel further away from fibres. (a) Images representing mutant. (b) Images representing WT. Black regions in the image indicate the presence of fibres. Visually, the wild type extracellular matrix shows smaller gaps and more frequent dark regions, indicating a denser presence of fibres and fewer bright areas. In contrast, the mutant images display larger, more prominent bright yellow regions, suggesting greater and more frequent separation between the fibres.*

The wild type also exhibits a broader range of fibre counts across the images, indicating greater variability. In contrast, the mutant fibroblasts appear to have a more consistent, predictable number of fibres, as they fall within a narrower range.

Mutants had a higher average relative gap size in comparison to the WT presented in (Table 1). The highest mutant value was 0.5542 and 0.5278 for WT. The lowest value for mutant was 0.5215 and WT was 0.4926. Therefore, WT had a bigger variance than the RBD (Fig. 6), interestingly the mean for WT was close to the highest value. Observing the visual representation of the gaps in (Fig. 5). The mutant culture images (Fig. 5a) have frequent regions with large intensities (yellow) indicating the presence of a larger number of large gaps in comparison to the WT images (Fig. 5b), where the presence of darker regions (black) is more common in comparison. Larger gaps in the mutant extracellular matrix suggest increased separation between the fibres, which may indicate a lower fibre density, and a less complex structural architecture compared to the wild type.

These results are inversely correlated, the greater the number of fibres that are present in the extra-cellular matrix, the smaller gaps that will occur. This was represented in [GRV19]. Fibronectin growth was observed with and without the addition of Ficoll, the addition of Ficoll grew more fibres of fibronectin which prompted smaller gaps.

3.2. Conclusions

In this paper, Trace Ridges was used to segment images from two different populations, mutant cells and wild type cells (WT). Trace Ridges was chosen for its robustness, accuracy, processing time and visualisation capabilities. DnCnn pre-processing filtering was employed to minimise noise and enhance features of the images. These segmentations were then used to explore the morphological features of the fibres and find characteristics that can distinguish between the two populations. Whilst these results were obtained with a relatively low number of images, they confirm that the Trace Ridges algorithm can be successfully used to compare the extracellular matrix of two different populations, and that there is a strong statistical difference for the two metrics extracted. Number of fibres exhibited a $p-value$ of 0.00091 and 0.014 for relative gap area size.

References

[ACACRA24] ARAFAT Y., CUESTA-APAUSA C., CASTELLANO E., REYES-ALDASORO C. C.: Fibre tracing in biomedical images: An objective comparison between seven algorithms. *submitted to biorxiv submitted to biorxiv* (Apr. 2024). 2, 3

[ACQ*20] ALIZADEH E., CASTLE J., QUIRK A., TAYLOR C. D., XU W., PRASAD A.: Cellular morphological features are predictive markers of cancer cell state. *Computers in Biology and Medicine 126* (Nov. 2020), 104044. URL: https://linkinghub.elsevier.com/retrieve/pii/S0010482520303759, doi:10.1016/j.compbiomed.2020.104044. 1

[Ber94] BERGUA A.: ["The Retina of the Vertebrates" by Santiago Ramón y Cajal–100 years in German translation]. *Klinische Monatsblatter Fur Augenheilkunde 205*, 6 (Dec. 1994), 372–373. doi:10.1055/s-2008-1045547. 1

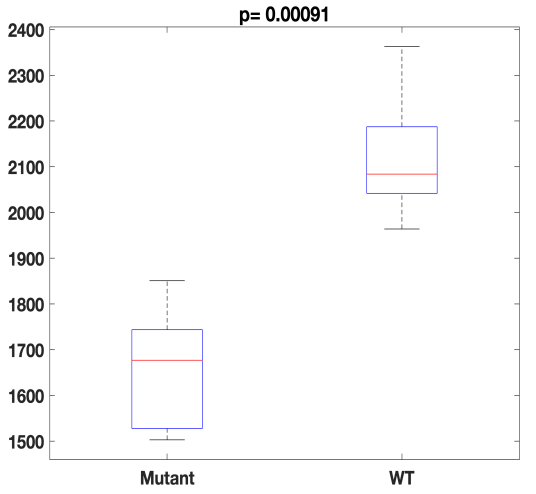

(a)

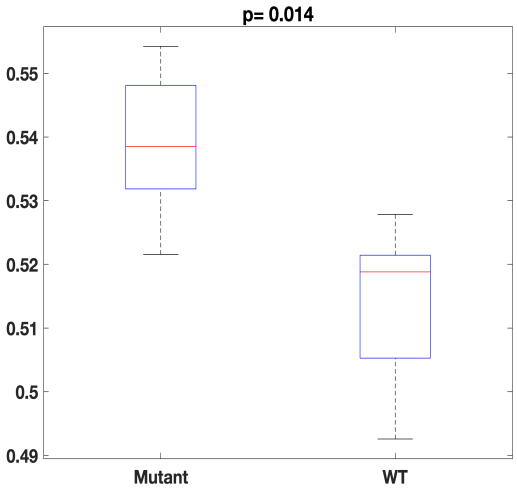

(b)

Figure 6: *Boxplots of morphological properties. (a) Number of edges with $p-value$ of* 0.00091 *(b) Gap Area with $p-value$ of* 0.014.

[BLP*14] BREDFELDT J. S., LIU Y., PEHLKE C. A., CONKLIN M. W., SZULCZEWSKI J. M., INMAN D. R., KEELY P. J., NOWAK R. D., MACKIE T. R., ELICEIRI K. W.: Computational segmentation of collagen fibers from second-harmonic generation images of breast cancer. *Journal of Biomedical Optics 19*, 1 (Jan. 2014), 016007. URL: https://www.ncbi.nlm.nih.gov/pmc/articles/PMC3886580/, doi:10.1117/1.JBO.19.1.016007. 2, 3

[Bra78] BRACEWELL R.: *The Fourier Transform and its Applications*, second ed. McGraw-Hill Kogakusha, Ltd., Tokyo, 1978. 3

[Can86] CANNY J.: A Comp. Approach to Edge Detection. *IEEE Trans PAMI 8*, 6 (1986), 679–698. 2, 4

[FCC18] FILIPE E. C., CHITTY J. L., COX T. R.: Charting the unexplored extracellular matrix in cancer. *International Journal of Experimental Pathology 99*, 2 (Apr. 2018), 58–76. URL: https://www.ncbi.nlm.nih.gov/pmc/articles/PMC6031881/, doi:10.1111/iep.12269. 2

[FDMJ10] FUKUMURA D., DUDA D. G., MUNN L. L., JAIN R. K.: Tumor microvasculature and microenvironment: novel insights through intravital imaging in pre-clinical models. *Microcirculation 17*, 3 (Apr. 2010), 206–25. doi:10.1111/j.1549-8719.2010.00029.x. 1

[GEOS*23] GRAPA A.-I., EFTHYMIOU G., OBBERGHEN-SCHILLING E. V., BLANC-FÉRAUD L., DESCOMBES X.: A spatial statistical framework for the parametric study of fiber networks: Application to fibronectin deposition by normal and activated fibroblasts. *Biological Imaging 3* (Jan. 2023), e25. doi:10.1017/S2633903X23000247. 2, 3

[Ges04] GEST H.: The discovery of microorganisms by Robert Hooke and Antoni Van Leeuwenhoek, fellows of the Royal Society. *Notes and Records of the Royal Society of London 58*, 2 (May 2004), 187–201. doi:10.1098/rsnr.2004.0055. 1

[Gra20] GRAPA A.-I.: *Characterization of fibronectin networks using graph-based representations of the fibers from 2D confocal images*. PhD thesis, Université Côte d'Azur, 2020. 2

[GRH*07] GUPTA S., RAMJAUN A. R., HAIKO P., WANG Y., WARNE P. H., NICKE B., NYE E., STAMP G., ALITALO K., DOWNWARD J.: Binding of ras to phosphoinositide 3-kinase p110alpha is required for ras-driven tumorigenesis in mice. *Cell 129*, 5 (June 2007), 957–968. doi:10.1016/j.cell.2007.03.051. 2

[GRV19] GRAHAM J., RAGHUNATH M., VOGEL V.: Fibrillar fibronectin plays a key role as nucleator of collagen I polymerization during macromolecular crowding-enhanced matrix assembly. *Biomaterials Science 7*, 11 (Oct. 2019), 4519–4535. Publisher: The Royal Society of Chemistry. URL: https://pubs.rsc.org/en/content/articlelanding/2019/bm/c9bm00868c, doi:10.1039/C9BM00868C. 6

[HLHL22] HU M., LI M., HUANG H., LU C.: Isolated cancer stem cells from human liver cancer: morphological and functional characteristics in primary culture. *Clinical & Translational Oncology: 24*, 1 (Jan. 2022), 48–56. doi:10.1007/s12094-021-02667-w. 1

[HS16] HEMALATHA G., SUMATHI C. P.: Preprocessing techniques of facial image with median and gabor filters. In *2016 International Conference on Information Communication and Embedded Systems (ICICES)* (2016), pp. 1–6. doi:10.1109/ICICES.2016.7518860. 3

[HZW*21] HUANG J., ZHANG L., WAN D., ZHOU L., ZHENG S., LIN S., QIAO Y.: Extracellular matrix and its therapeutic potential for cancer treatment. *Signal Transduction and Targeted Therapy 6*, 1 (Apr. 2021), 1–24. Publisher: Nature Publishing Group. URL: https://www.nature.com/articles/s41392-021-00544-0, doi:10.1038/s41392-021-00544-0. 1

[IG18] IOZZO R. V., GUBBIOTTI M. A.: Extracellular Matrix: The driving force of mammalian diseases. *Matrix biology : journal of the International Society for Matrix Biology 71-72* (Oct. 2018), 1–9. URL: https://www.ncbi.nlm.nih.gov/pmc/articles/PMC6146050/, doi:10.1016/j.matbio.2018.03.023. 2

[II21] ILESANMI A. E., ILESANMI T. O.: Methods for image denoising using convolutional neural network: a review. *Complex & Intelligent Systems 7*, 5 (Oct. 2021), 2179–2198. URL: https://doi.org/10.1007/s40747-021-00428-4, doi:10.1007/s40747-021-00428-4. 3

[Lin98a] LINDEBERG T.: Edge detection and ridge detection with automatic scale selection. *Int J Comp Vision 30*, 2 (Nov. 1998), 117–154. URL: ://000077990700002. 2

[Lin98b] LINDEBERG T.: Feature detection with automatic scale selection. *Int J Comp Vision 30*, 2 (Nov. 1998), 79–116. URL: ://000077990700001. 2

[LKP*20] LIU Y., KEIKHOSRAVI A., PEHLKE C. A., BREDFELDT J. S., DUTSON M., LIU H., MEHTA G. S., CLAUS R., PATEL A. J., CONKLIN M. W., INMAN D. R., PROVENZANO

P. P., SIFAKIS E., PATEL J. M., ELICEIRI K. W.: Fibrillar Collagen Quantification With Curvelet Transform Based Computational Methods. *Frontiers in Bioengineering and Biotechnology 8* (2020). URL: https://www.frontiersin.org/articles/10.3389/fbioe.2020.00198. 2, 3

[Mey92] MEYER F. S. B.: The Morphological Approach to Segmentation: The Watershed Transformation. In *Mathematical Morphology in Image Processing*. CRC Press, 1992. Num Pages: 49. 2, 4

[Mey94] MEYER F.: Topographic distance and watershed lines. *Signal Processing 38*, 1 (July 1994), 113–125. URL: https://www.sciencedirect.com/science/article/pii/0165168494900604, doi:10.1016/0165-1684(94)90060-4. 2, 4

[MSMB21] MOUSAVIKHAMENE Z., SYKORA D. J., MRKSICH M., BAGHERI N.: Morphological features of single cells enable accurate automated classification of cancer from non-cancer cell lines. *Scientific Reports 11*, 1 (Dec. 2021), 24375. URL: https://www.nature.com/articles/s41598-021-03813-8, doi:10.1038/s41598-021-03813-8. 1

[MWCU20] MCQUITTY C. E., WILLIAMS R., CHOKSHI S., URBANI L.: Immunomodulatory Role of the Extracellular Matrix Within the Liver Disease Microenvironment. *Frontiers in Immunology 11* (Nov. 2020). Publisher: Frontiers. URL: https://www.frontiersin.org/journals/immunology/articles/10.3389/fimmu.2020.574276/full, doi:10.3389/fimmu.2020.574276. 1

[PJ22] POPOVA N. V., JÜCKER M.: The Functional Role of Extracellular Matrix Proteins in Cancer. *Cancers 14*, 1 (Jan. 2022), 238. doi:10.3390/cancers14010238. 1

[PLG*21] POMPILI S., LATELLA G., GAUDIO E., SFERRA R., VETUSCHI A.: The Charming World of the Extracellular Matrix: A Dynamic and Protective Network of the Intestinal Wall. *Frontiers in Medicine 8* (Apr. 2021), 610189. URL: https://www.ncbi.nlm.nih.gov/pmc/articles/PMC8085262/, doi:10.3389/fmed.2021.610189. 2

[PMFT02] PUPA S. M., MÉNARD S., FORTI S., TAGLIABUE E.: New insights into the role of extracellular matrix during tumor onset and progression. *Journal of Cellular Physiology 192*, 3 (Sept. 2002), 259–267. URL: https://onlinelibrary.wiley.com/doi/10.1002/jcp.10142, doi:10.1002/jcp.10142. 1

[RFB15] RONNEBERGER O., FISCHER P., BROX T.: U-Net: Convolutional Networks for Biomedical Image Segmentation. In *Medical Image Computing and Computer-Assisted Intervention – MICCAI 2015* (Cham, 2015), Navab N., Hornegger J., Wells W. M., Frangi A. F., (Eds.), Springer International Publishing, pp. 234–241. doi:10.1007/978-3-319-24574-4_28. 2

[RH99] RANDEN T., HUSOY J.: Filtering for texture classification: a comparative study. *IEEE Transactions on Pattern Analysis and Machine Intelligence 21*, 4 (1999), 291–310. doi:10.1109/34.761261. 3

[SV17] SUHAS S., VENUGOPAL C. R.: Mri image preprocessing and noise removal technique using linear and nonlinear filters. In *2017 International Conference on Electrical, Electronics, Communication, Computer, and Optimization Techniques (ICEECCOT)* (2017), pp. 1–4. doi:10.1109/ICEECCOT.2017.8284595. 3

[WAOMW20] WINKLER J., ABISOYE-OGUNNIYAN A., METCALF K. J., WERB Z.: Concepts of extracellular matrix remodelling in tumour progression and metastasis. *Nature Communications 11*, 1 (Oct. 2020), 5120. Publisher: Nature Publishing Group. URL: https://www.nature.com/articles/s41467-020-18794-x, doi:10.1038/s41467-020-18794-x. 1

[WMDRH18] WALKER C., MOJARES E., DEL RÍO HERNÁNDEZ A.: Role of Extracellular Matrix in Development and Cancer Progression. *International Journal of Molecular Sciences 19*, 10 (Oct. 2018), 3028. doi:10.3390/ijms19103028. 1

[WPB*21] WERSHOF E., PARK D., BARRY D. J., JENKINS R. P., RULLAN A., WILKINS A., SCHLEGELMILCH K., ROXANIS I., ANDERSON K. I., BATES P. A., SAHAI E.: A FIJI macro for quantifying pattern in extracellular matrix. *Life Science Alliance 4*, 3 (Mar. 2021). Publisher: Life Science Alliance Section: Methods. URL: https://www.life-science-alliance.org/content/4/3/e202000880, doi:10.26508/lsa.202000880. 2, 3

[WPK*15] WU P.-H., PHILLIP J. M., KHATAU S. B., CHEN W.-C., STIRMAN J., ROSSEEL S., TSCHUDI K., VAN PATTEN J., WONG M., GUPTA S., BARAS A. S., LEEK J. T., MAITRA A., WIRTZ D.: Evolution of cellular morpho-phenotypes in cancer metastasis. *Scientific Reports 5*, 1 (Dec. 2015), 18437. Publisher: Nature Publishing Group. URL: https://www.nature.com/articles/srep18437, doi:10.1038/srep18437. 1

[YCH*24] YAO J., CHEN Y., HUANG Y., SUN X., SHI X.: The role of cardiac microenvironment in cardiovascular diseases: implications for therapy. *Human Cell 37*, 3 (May 2024), 607–624. URL: https://doi.org/10.1007/s13577-024-01052-3, doi:10.1007/s13577-024-01052-3. 1

[Yue14] YUE B.: Biology of the Extracellular Matrix: An Overview. *Journal of glaucoma* (2014), S20–S23. URL: https://www.ncbi.nlm.nih.gov/pmc/articles/PMC4185430/, doi:10.1097/IJG.0000000000000108. 2

[ZZC*17] ZHANG K., ZUO W., CHEN Y., MENG D., ZHANG L.: Beyond a Gaussian Denoiser: Residual Learning of Deep CNN for Image Denoising. *IEEE Transactions on Image Processing 26*, 7 (July 2017), 3142–3155. URL: https://ieeexplore.ieee.org/document/7839189/, doi:10.1109/TIP.2017.2662206. 3